Scripta Materialia 171 (2019) 112–117

Contents lists available at ScienceDirect

Scripta Materialia

journal homepage: www.elsevier.com/locate/scriptamat

Martensite variant localization effects on fatigue crack growth - The CuZnAl example

J. Yaacoub [a], Y. Wu [a], W. Abuzaid [b], D. Canadinc [a,c], H. Sehitoglu [a,*]

[a] Department of Mechanical Science and Engineering, University of Illinois at Urbana-Champaign, 1206 W. Green St., Urbana, IL 61801, USA
[b] Department of Mechanical Engineering, American University of Sharjah, PO Box 26666, Sharjah, United Arab Emirates
[c] Advanced Materials Group (AMG), Department of Mechanical Engineering, Koç University, 34450 Istanbul, Turkey

ARTICLE INFO

Article history:
Received 30 May 2019
Received in revised form 24 June 2019
Accepted 25 June 2019
Available online xxxx

Keywords:
Stress induced martensite
Crack opening displacement
Superelasticity
CuZnAl
Fatigue crack growth

ABSTRACT

The paper underscores the difficulty in characterizing crack growth in shape memory alloys with conventional stress intensity approaches even when anisotropy is accounted for. The local displacements deviate significantly from the presumed K solutions because of transformation localization at macro scales extending from the crack tip. Modifications in stress intensity due to variant induced tractions are derived providing an explanation of the extrinsic behavior. Precise displacement and strain measurements are provided to highlight the complexity of deformation and the need for better fracture mechanics models, including crack tip opening displacements, to characterize fatigue crack growth in shape memory alloys.

Intense research focused on shape memory alloys (SMA) has improved our fundamental understanding of this class of materials. These efforts have enabled the development of specific and unique applications exploiting their shape memory and superelastic properties. Near equiatomic NiTi continues to be the most popular and well-studied shape memory alloy exhibiting large transformation strains and relatively superior fatigue properties. CuZnAl constitutes an attractive and cost-effective alternative to NiTi, but is not widely utilized [1–3], in part due to the relatively limited understanding of its fatigue properties [4], and partly due to martensite stabilization [5]. In single crystalline form, CuZnAl exhibits a very stable response with excellent levels of transformation strains even exceeding that of NiTi. In addition, CuZnAl is promising due to the large gap between the transformation stress and slip (plasticity) stress levels. This large gap contributes to stable response over many cycles and consequently limits the degradation under cyclic loading conditions [6–8]. Moreover, CuZnAl can exhibit superelasticity over a higher temperature range as compared to NiTi [9]. It is therefore foreseeable for CuZnAl to be implemented in various engineering applications [10,11]. This, however, warrants a good understanding of the fatigue behavior and the corresponding microstructure of the CuZnAl alloy, which is being addressed in this paper.

SMAs subject to cyclic loading may experience incremental degradation in the transformation strains accompanied by the accumulation of permanent and irrecoverable deformation. The microstructural mechanisms responsible for this deterioration of superelastic properties, typically referred to as functional fatigue, are still subject to debate and require further research. Nevertheless, localized plasticity and the build-up of dislocations at the transformation front have been widely discussed as a major driving force [12,13]. In addition to cyclic degradation and functional fatigue, SMAs exhibit a rather complex crack growth behavior influenced by phase transformation at the crack tip. Conventional fracture mechanics approaches have been typically used to describe the fatigue crack growth response of SMAs at the macroscale. This approach has served the community well, however, it does not account for the stress induced martensitic transformation ahead of the crack tip, a unique characteristic of superelastic SMAs. In turn, the quantification of stress intensity factor under such conditions is not satisfactory. Efforts to address this limitation have employed novel methods to quantify the effective crack tip stress intensity factor accounting for stress induced transformation ahead of the crack tip in Ni_2FeGa and NiTi [14–16]. It is worth noting that in all the aforementioned studies, where applicable, symmetric and homogeneous deformation around the crack tip was reported.

In contrast to NiTi, the fatigue crack growth behavior of CuZnAl exhibits a high-strain transformation band at the crack tip at macroscales. This response is thought to be triggered by the high elastic anisotropy of CuZnAl [1] compared to NiTi, which is manifested by the activation of a dominant martensite variant, preferentially on one half of the crack plane. These localization effects are relevant to our understanding of fatigue thresholds, defined as the limit above which critical crack growth rates are observed, and the subcritical Paris law regime. The

* Corresponding author.
E-mail address: huseyin@illinois.edu (H. Sehitoglu).

https://doi.org/10.1016/j.scriptamat.2019.06.032
1359-6462/

purpose of the present work is to draw attention to this localization observed in CuZnAl single crystals.

We report fatigue crack growth results where we measure the strain and displacement fields near the crack tip, from which the crack tip opening displacements and the stress intensity ranges are extracted. The results correlate well with the crack tip opening displacements for two different CuZnAl crystal orientations. On the other hand, the stress intensity range calculation must incorporate the martensite variant localization. The paper points to the need to understand the complexity of the crack tip displacement fields, which are highly non-uniform and deviate from anisotropic elasticity solutions.

The current investigation considers two single crystals of [001] and [011] orientations, both of composition 59.2 at.% Cu, 27 at.% Zn and 13.8 at.% Al. The samples were solutionized at 800 °C for 30 min followed by water quenching and were then heat-treated at 80 °C for 24 h after which they are air-cooled. The transformation temperatures are determined as $A_s = 4$ °C, $A_f = 13$ °C, $M_s = 1$ °C, $M_f = -12.5$ °C by Differential Scanning Calorimetry (DSC). The martensite for this composition has an 18R crystal structure [17] and the corresponding elastic constants are given in [18]. The crystallographic orientations were verified using EBSD (Electron Backscatter Diffraction). The dog-bone shaped specimens had a gauge section of 10 mm length, 1.5 mm thickness and 3 mm width, and featured 0.5 mm edge notches introduced using EDM. Prior to loading, all specimens were polished using SiC paper, after which a fine speckle pattern was applied for full-field strain measurements using Digital Image Correlation (DIC) [19]. Uniaxial tension experiments were conducted on a servo-hydraulic load frame equipped with a digital controller. The stress-strain curves shown with a solid line in Fig. 1 demonstrate the global sample response with the strains extracted from the entire gauge section of the sample, and the dashed blue curves represent the local responses based on specific locations on the samples' gauge sections, where the strains were localized and attained maximal values. Both global and local stress-strain curves point to complete strain recovery upon unloading with very limited plastic deformation, as well as the orientation dependence of the superelastic behavior.

Fatigue crack growth experiments were conducted with an R ratio of 0.05 and 3 Hz frequency, and at a temperature of 40 °C, employing constant stress amplitudes of 95 MPa and 66.5 MPa for the [011] and [001] orientations, respectively. A representative loading cycle is

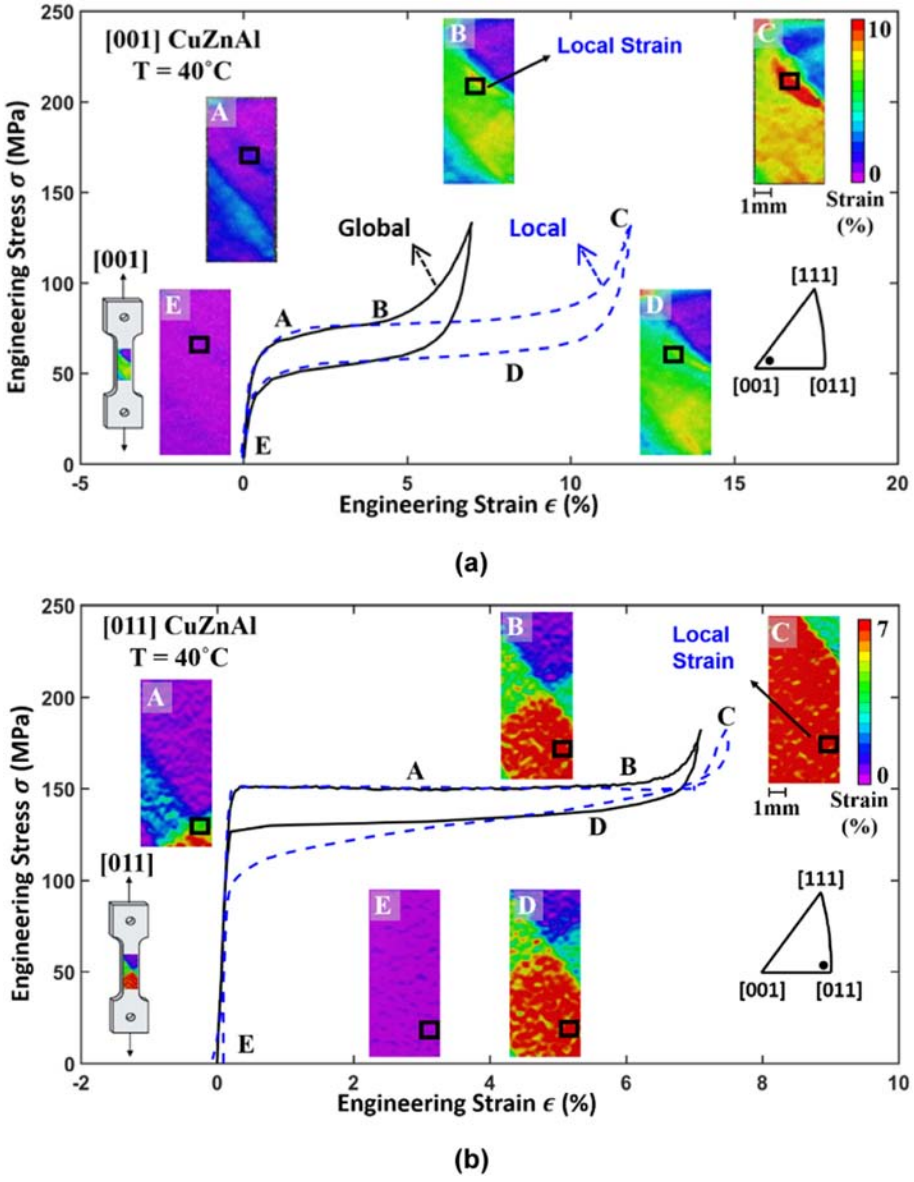

Fig. 1. Stress strain response of the (a) [001] and (b) [011] single crystals. Solid black and dashed blue lines represent global and local responses, respectively. Note the different strain scales of (a) and (b). (For interpretation of the references to color in this figure legend, the reader is referred to the web version of this article.)

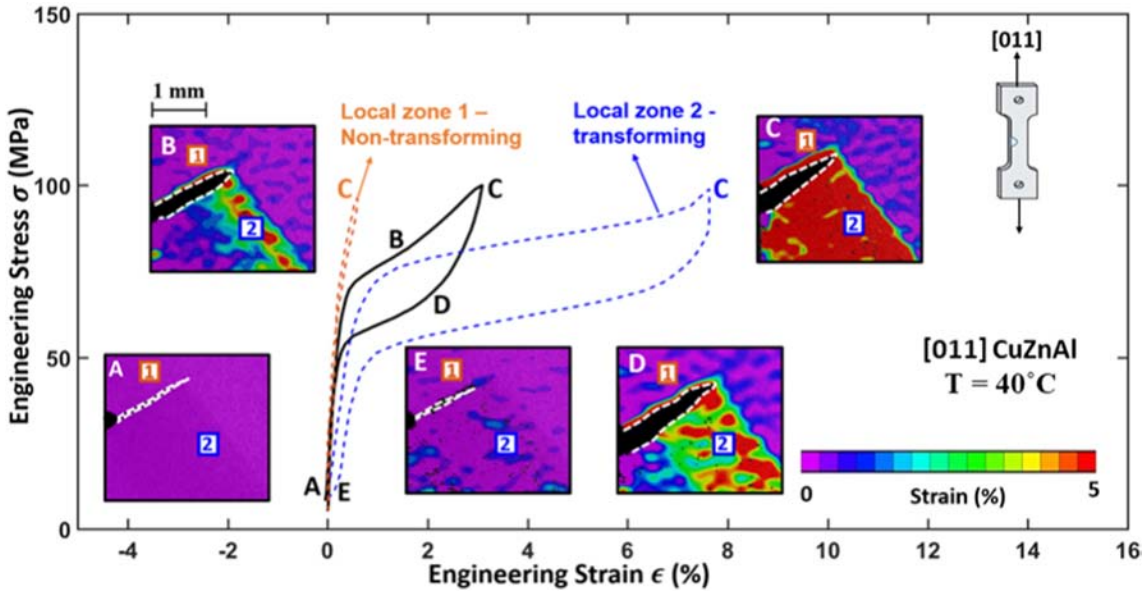

Fig. 2. Representative deformation cycle of a [011]-oriented sample subject to fatigue loading. The solid black line represents the global stress-strain response. Boxes 1 (orange) and 2 (blue) represent the locations at which the local stress-strain response is plotted using dashed lines. (For interpretation of the references to color in this figure legend, the reader is referred to the web version of this article.)

presented in Fig. 2 for the [011] orientation. Optical images were collected during each loading cycle allowing for the extraction of displacement fields, from which the stress intensity factor was calculated via regression analysis based on anisotropic elasticity solutions as explained in [14]. Strain contour plots at different stages along the loading curve are presented as insets. The blue and orange dashed lines represent the local strain levels at two different locations around the crack; transforming and non-transforming, respectively. These locations are outlined in the strain contour plots shown as insets in Fig. 2. Accordingly, zone 1 deforms only elastically, while zone 2 exhibits large strains of almost 8%, associated with stress induced martensitic transformation. This localization results in asymmetric opening of the crack.

The high-resolution digital image correlation analysis permitted the study of local strains, as well as displacement fields in the vicinity of the cracks. The variants that form at the crack tip differ from those that form at the initial notch. These findings point to the need to carefully analyze the variants that form and are ultimately responsible for crack advance. We note that crack nucleation occurs at the austenite-martensite interfaces after which the fatigue crack creates its own preferred variant emanating from the crack tip and extending in its wake. This is similar to a Lüder's band observed in metals. The local strains in the transformed band are near 8% as illustrated in Fig. 3(a).

We note that, because of the presence of the transformation band, the displacement contours are not symmetric with respect to the crack's center line. Experimentally measured vertical displacement contours are plotted in Fig. 3(b) with a level step of 3 μm. It is obvious that, with respect to the crack, the contour lines below are denser and carry higher magnitudes than those above. Fig. 3(b) also shows the same contours with the anisotropic regression solutions superimposed. A detailed explanation of the procedure for anisotropic regression is provided in [14]. The solutions fit well with the experimental contour lines in the non-transforming region on top of the crack (levels 3, 6 and 9 in Fig. 3(b)), but fail to capture the behavior of the transformation band at the bottom as the theoretical crack tip displacement fields used in regression are obtained from anisotropic elasticity theory and do not account for transformation in the vicinity of the fatigue crack [20]. This explains the agreement of the solutions with the top side of the crack, non-transforming and elastic, and not the bottom, which is undergoing transformation. Such a solution with biased displacement fields provides the stress intensity that matches the fracture mechanics solution modified with the effect of internal tractions as described herein.

The correlation of the results with crack tip opening displacement and stress intensity factor ranges is provided in Fig. 4: CuZnAl alloys exhibit threshold values for both crack opening displacement and stress intensity level. The fatigue crack growth rates correlate particularly well with the crack opening displacement range, as seen in Fig. 4(b). This is rather important because the crack tip opening displacement is experimentally measured while the anisotropic stress intensity solution normalizes the experimentally observed localization effects. The results also point to the absence of a unique threshold stress intensity value for the two crystal orientations considered: 4.8 as compared to 9 MPa$\sqrt{m}$ for [001] and [011], respectively. In contrast, the threshold crack tip opening displacement seems to be unique exhibiting the same magnitude for both orientations at 4 μm. Moreover, we note the ramifications of asymmetric opening displacements at crack tips. Because the fatigue crack front can slide in the direction of the transforming band, large displacements can develop which facilitate crack growth. These findings seem intuitive and the experiments concur.

The extrinsic factors (shielding effects) that impart fatigue crack growth resistance are well known. On the other hand, extrinsic factors that reduce the resistance are not as well understood. The latter effect can be classified as a deshielding effect (transformation aiding the crack growth): we calculate the change of driving force due to the asymmetric transformation in [011] CuZnAl case. The internal forces within the transformation domain generate local Mode I and Mode II components adding to the external stress (Fig. 4(c)). The calculation relies on weight functions for anistropic media and Eshelby's inclusion method [21]: using weight function theory [22], the stress intensity, ΔK_{Change}, associated with the internal tractions on the transformation zone can be obtained. The details of the weight function/Eshelby based calculation procedure are elucidated in [23]. The modified da/dN vs. ΔK plot is presented in Fig. 4(c) where the black dots are acquired from classical handbook solution [24], ΔK_{LEFM}, the blue dots represent the same cases presented in Fig. 4(a), $\Delta K_{Regression}$, and the red dots are the superposition of ΔK_{LEFM} and ΔK_{Change}. We note the excellent agreement between

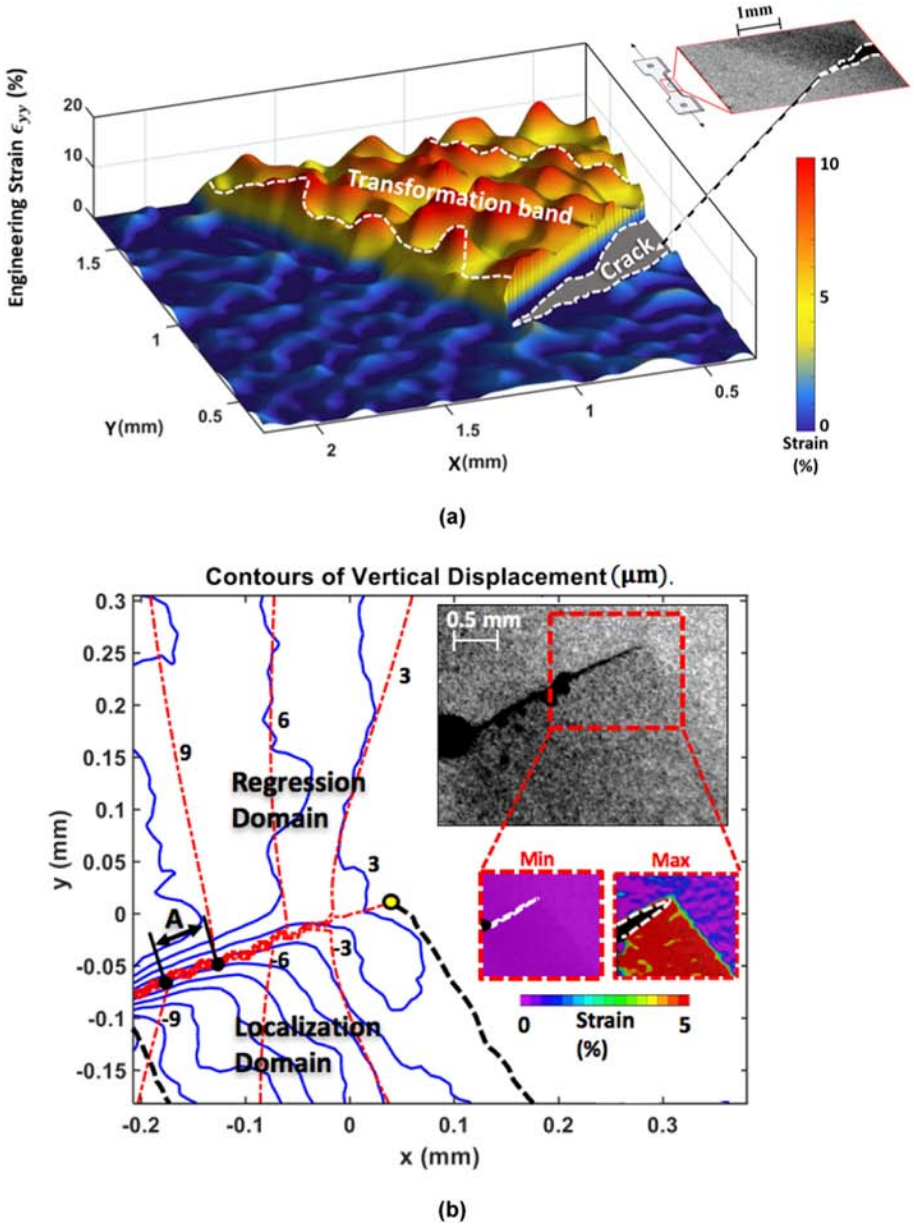

Fig. 3. The case of [011] orientation: (a) Normal strain around the crack (b) experimental vertical contour lines (blue) with anisotropic regression overlay. Note the shift in displacement contours (A) across the crack faces due to anisotropy. (For interpretation of the references to color in this figure legend, the reader is referred to the web version of this article.)

$\Delta K_{Regression}$ and $\Delta K_{LEFM} + \Delta K_{Change}$. The positive ΔK_{Change} contribution due to the asymmetric transformation at the crack tip reduces the external loading capacity (i.e. small ΔK_{LEFM}). This is a vital observation in the assessment of shape memory alloys, in general.

The results further show that the transformation zones do not conform to the transformation zones in NiTi or Ni_2FeGa [25–29]. This evidences the complexity of the driving forces in the case of asymmetrically transforming SMAs, pointing to the need to understand localization of variants at the crack tip, as it leads to deviations from classical and non-transforming crack tip analysis. Simple solutions of crack tip fields will not capture the complexity that arises due to the localization of the transformation. While the stress intensity or other energy release rate solutions are still at their infancy, the crack tip opening displacement provides a convincing driving force parameter.

We draw attention to the role of Critical Resolved Shear Stress (CRSS) of stress induced transformation on the results. The plastic flow can be influenced by the non-Schmid behavior of CuZnAl, where the transformation is a strong function of the stress state as recently illustrated in [17]: in the current work, the [001] and [011] orientations exhibit different transformation stress levels (Fig. 1). Using the habit planes, we can calculate the Schmid factors and evaluate the corresponding CRSS for transformation. The Schmid factor for the most favored variant is 0.48 and 0.45 for the [001] and [011] orientations while the CRSS values are 25 and 45 MPa, respectively. Inevitably, the role of different flow stresses contributes to the differences in the threshold levels shown in Fig. 4(a). Further work is needed to develop a model that incorporates the crystalline texture dependence of the fatigue threshold levels.

Fatigue crack growth literature has made a distinction between thresholds obtained from long and short cracks. The short crack threshold corresponds to activation of a Stage I crack where shearing along crystallographic plane(s) occurs. On the other hand, the long crack threshold is obtained for a Stage II crack where advancement occurs by plastic flow in a homogenized media. It is the Stage I crack with

localized transformation in this case that is considered in this work. Since the majority of fatigue life corresponds to growth of small flaws, this regime is deemed to be the most relevant.

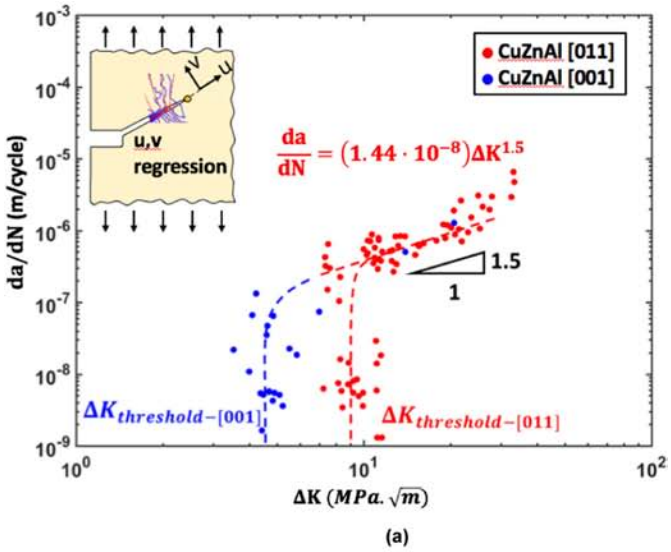

(a)

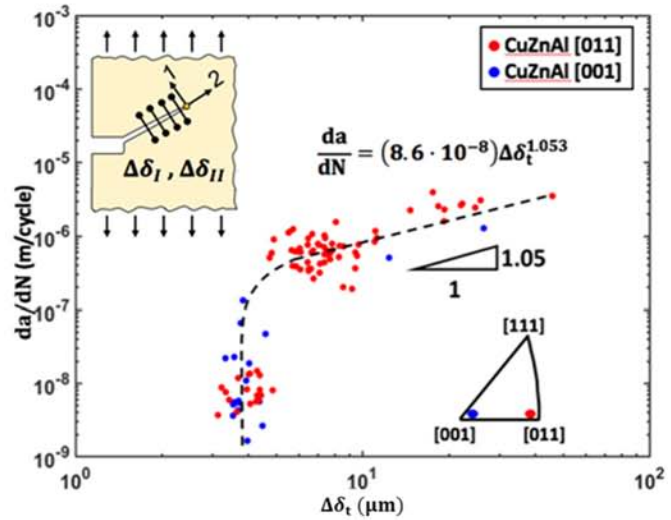

(b)

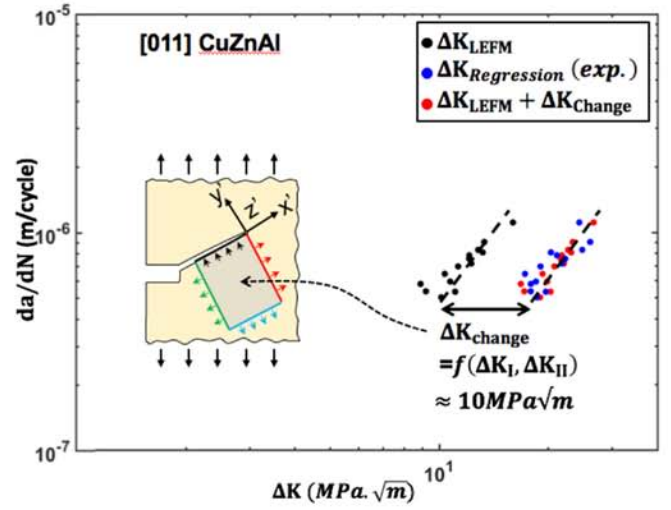

(c)

Overall, the work presented herein supports the following conclusions:

(1) Crack nucleation occurs at the austenite-martensite interface of the most favorably oriented martensite variant. Once the crack initiates and the crack advances, it creates its own favorably oriented variant which differs from the variant that initially nucleated. The localization associated with the crack tip growth variant creates highly non-symmetric displacement and strain fields.
(2) The results point to a non-unique threshold value for fatigue crack growth, which depends on orientations of preferred variants and the critical transformation stress levels, which themselves are orientation dependent.
(3) The crack tip opening displacement range represents a physically measured parameter that correlates well with the fatigue crack growth rates, and stress intensity range was included for comparison. However, further work is needed to develop energy release rate parameters incorporating the localization behavior in these classes of alloys.
(4) The external loading capacity of CuZnAl drastically deteriorates due to a positive K contribution resulting from the asymmetric transformation behavior at the crack tip (deshielding effect).

Acknowledgement

This work is funded by the National Science Foundation DMR grant 1709515 Metallic Materials and Nanomaterials Program. The EBSD analyses were carried out in part in the Frederick Seitz Materials Research Laboratory Central Research Facilities, University of Illinois. The single crystals were grown by Prof. Yuriy Chumlyakov, Tomsk State University, Russia.

References

[1] H. Sakamoto, Y. Kijima, K. Shimizu, ichi rsquo, Trans. Jpn. Inst. Metals 23 (10) (1982) 585–594.
[2] K.N. Melton, O. Mercier, Scr. Metall. 13 (1) (1979) 73–75.
[3] L. Delaey, J. Janssen, D. Van de Mosselaer, G. Dullenkopf, A. Deruyttere, Scr. Metall. 12 (4) (1978) 373–376.
[4] A. Yawny, F.C. Lovey, M. Sade, Mater. Sci. Eng. A 290 (1) (2000) 108–121.
[5] A.A. Arab, M. Ahlers, Acta Metall. 36 (9) (1988) 2627–2638.
[6] F.d.C. Bubani, M. Sade, F. Lovey, Mater. Sci. Eng. A 543 (2012) 88–95.
[7] T. Saburi, C.M. Wayman, K. Takata, S. Nenno, Acta Metall. 28 (1) (1980) 15–32.
[8] G. Wang, Eng. Fract. Mech. 46 (6) (1993) 909–930.
[9] Y. Wu, E. Ertekin, H. Sehitoglu, Acta Mater. 135 (2017) 158–176.
[10] J. Van Humbeeck, J. Alloys Compd. 355 (1) (2003) 58–64.
[11] K. Otsuka, C.M. Wayman, Shape Memory Materials, Cambridge University Press, 1999.
[12] M. Sade, C. Damiani, R. Gastien, F.C. Lovey, J. Malarría, A. Yawny, Smart Mater. Struct. 16 (1) (2007) S126.
[13] P. Sedmák, P. Šittner, J. Pilch, C. Curfs, Acta Mater. 94 (2015) 257–270.
[14] Y. Wu, A. Ojha, L. Patriarca, H.J. Maier, H. Sehitoglu, Shape Memory and Superelasticity 1 (1) (2015) 18–40.
[15] C. Maletta, E. Sgambitterra, F. Niccoli, Sci. Rep. 6 (1) (2016) 17.
[16] E. Sgambitterra, C. Maletta, F. Furgiuele, H. Sehitoglu, Int. J. Fatigue 112 (2018) 9–20.
[17] S. Alkan, Y. Wu, A. Ojha, H. Sehitoglu, Acta Mater. 149 (2018) 220–234.
[18] P.L. Rodriguez, F.C. Lovey, G. Guenin, J.L. Pelegrina, M. Sade, M. Morin, Acta Metall. Mater. 41 (11) (1993) 3307–3310.
[19] J.R. Yates, M. Zanganeh, Y.H. Tai, Eng. Fract. Mech. 77 (11) (2010) 2063–2076.
[20] G.C. Sih, P.C. Paris, G. Irwin, Int. J. Frac. Mech. 1 (3) (1965) 189–203.
[21] J.D. Eshelby, Proc. R. Soc. Lond. A Math. Phys. Sci. 241 (1226) (1957) 376–396.
[22] J.R. Rice, Int. J. Solids Struct. 8 (6) (1972) 751–758.
[23] Y. Wu, J. Yaacoub, F. Brenne, W. Abuzaid, D. Canadinc, H. Sehitoglu, Acta Mater. (2019)https://doi.org/10.1016/j.actamat.2019.06.042.

Fig. 4. (a) Stress intensity range analysis (b) crack tip opening displacement analysis (c) illustration of stress intensity factor change due to internal tractions. In (c) the black dots demonstrate the results from the handbook (LEFM), blue dots the regression results, and the red dots the combination of handbook results with the calculated ΔK_{change}. The dashed lines are added to aid the eye. (For interpretation of the references to color in this figure legend, the reader is referred to the web version of this article.)

[24] H. Tada, P. Paris, G. Irwin, The Stress Analysis of Cracks Handbook, 2, ASME Press, New York, 2000 1.
[25] M.R. Laydi, C. Lexcellent, Shape Memory and Superelasticity 1 (3) (2015) 339–346.
[26] C. Maletta, F. Furgiuele, Acta Mater. 58 (1) (2010) 92–101.
[27] C. Maletta, M. Young, J. Mat. Eng. Perf. 20 (2011) 597.
[28] S. Gollerthan, M.L. Young, A. Baruj, J. Frenzel, W.W. Schmahl, G. Eggeler, Acta Mater. 57 (4) (2009) 1015–1025.
[29] S. Gollerthan, M.L. Young, K. Neuking, U. Ramamurty, G. Eggeler, Acta Mater. 57 (19) (2009) 5892–5897.